Instabilities in a free granular fluid described by the Enskog equation

Vicente Garzó*
Departamento de Física, Universidad de Extremadura, E-06071 Badajoz, Spain
(Received 28 February 2005; published 25 August 2005)

A linear stability analysis of the hydrodynamic equations with respect to the homogeneous cooling state is carried out to identify the conditions for stability as functions of the wave vector, the dissipation, and the density. In contrast to previous studies, this description is based on the results derived from the Enskog equation for inelastic hard spheres [V. Garzó and J. W. Dufty, Phys. Rev. E **59**, 5895 (1999)], which takes into account the dependence of the transport coefficients on dissipation. As expected, linear stability shows two transversal (shear) modes and a longitudinal ("heat") mode to be unstable with respect to long enough wavelength excitations. Comparison with previous results (which neglect the influence of dissipation on transport) shows quantitative discrepancies for strong dissipation.

DOI: 10.1103/PhysRevE.72.021106 PACS number(s): 05.20.Dd, 45.70.Mg, 51.10.+y, 47.50.+d

I. INTRODUCTION

A simple way of capturing the dynamics of granular media under rapid flow conditions is through an idealized fluid of smooth, inelastic hard spheres. The inelasticity of collisions is only accounted for by a (constant) coefficient of normal restitution $0<\alpha\leq 1$ that only affects the translational degrees of freedom of grains. Despite the simplicity of the model, it has been widely used as a prototype to understand some of the physical mechanisms involved in granular flows, especially those related to the inelasticity of granular collisions. In particular, one of the most characteristic features of granular fluids, as compared with normal fluids, is the spontaneous formation of velocity vortices and density clusters when evolving freely. This clustering instability can be well described through a linear stability analysis of the hydrodynamic equations and follows from the presence of a dissipation term in the equation for the balance of energy. An important feature of this instability is that it is confined to long wavelengths (small wave numbers) and so it can be avoided for small enough systems. Detected by Goldhirsch and Zanetti [1] and McNamara [2], the clustering problem has attracted much attention in the past few years, especially from a computational point of view [3].

In the case of a low-density gas, accurate predictions for the unstable hydrodynamic modes have been made from the (inelastic) Boltzmann equation [4–6]. In particular, a critical length L_c is identified, so that the system becomes unstable when its linear size is larger than L_c. The dependence of L_c on the coefficient of restitution α predicted by kinetic theory compares quite well with numerical results obtained by using the direct simulation Monte Carlo method [7].

For finite higher densities, these instabilities have been studied by several authors using macroscopic or kinetic equations [1,2,8]. A careful study of the dispersion relations has been recently carried out by van Noije and Ernst [9] from the Enskog kinetic theory but neglecting any dependence of the pressure and of the transport coefficients on inelasticity. Specifically, they assume that the expressions for the hydrostatic pressure, the shear viscosity, the bulk viscosity, and the thermal conductivity are the same as those for the *elastic* gas [10], except that the temperature still depends explicitly on time to account for the homogenous cooling. However, given that the effect of inelasticity on dense fluid transport is quite important in the undriven case [11,12] (see for instance, Fig. 1 below) the assumptions made in Ref. [9] could be only justified for very small dissipation (say for instance, $\alpha \approx 0.99$).

Although the predictions made by van Noije and Ernst [9] compares reasonably well with molecular dynamics simulation results, it is worth to assess to what extent the previous results [9] are indicative of what happens when the improved expressions for the *inelastic* transport coefficients are considered [11]. For this reason, in this paper I revisit the (unstable) hydrodynamic-mode problem of a granular fluid described by the *inelastic* Enskog kinetic theory [13]. In spite of the explicit knowledge of the Enskog transport coefficients [11], I am not aware of any previous solution of the linearized hydrodynamic equations for a moderately dense granular gas.

The Enskog kinetic equation can be considered as the extension of the Boltzmann equation to finite densities. As happens for elastic collisions, the inelastic Enskog equation provides a semiquantitative description of the hard sphere system that neglects the effects of correlations between the velocities of the two particles that are about to collide (molecular chaos assumption). The Enskog approximation is expected to be valid for short times since as the system evolves corrections to the Enskog equation due to multiparticle collisions, including recollision events ("ring" collisions) should be incorporated. The latter are expected to be stronger for fluids with inelastic collisions where the colliding pairs tend to be more focused. Therefore some deviations from molecular chaos have been observed in molecular dynamics (MD) simulations [14] of granular fluids as the density increases. Although the existence of these correlations restricts the range of validity of the Enskog equation, the latter can be still considered as a good approximation especially at the level of macroscopic properties (such as transport coefficients). In particular, the Enskog results presents quite a good

*Email address: vicenteg@unex.es

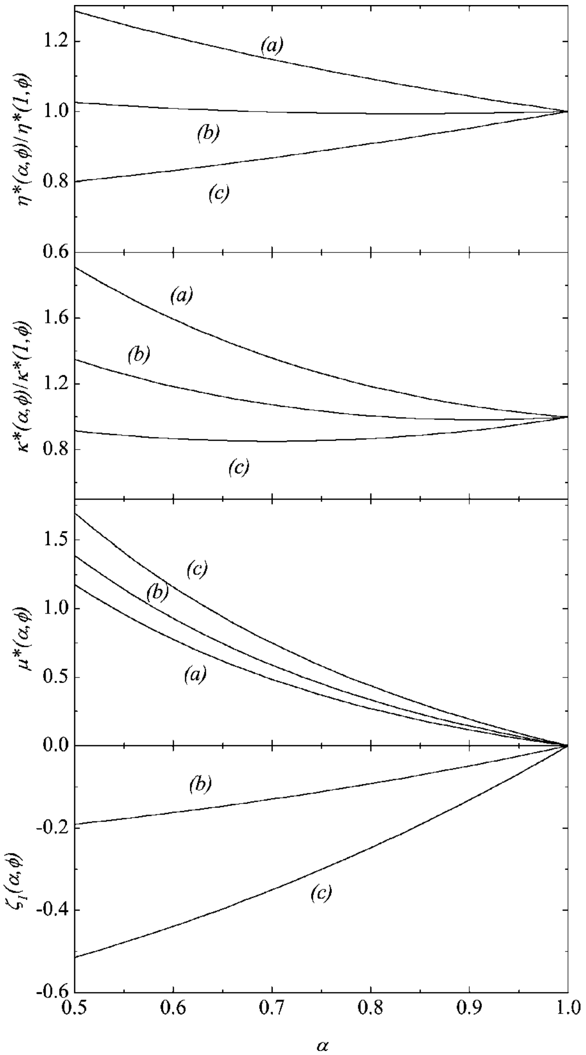

FIG. 1. Plot of $\eta^*(\alpha,\phi)/\eta^*(1,\phi), \kappa^*(\alpha,\phi)/\kappa^*(1,\phi), \mu^*(\alpha,\phi)$, and $\zeta_1(\alpha,\phi)$ versus the coefficient of restitution α for three different values of the solid volume fraction ϕ: (a) $\phi=0$, (b) $\phi=0.1$, and (c) $\phi=0.2$. Note that $\zeta_1=0$ at $\phi=0$.

agreement with MD simulations and even with real experiments. In the case of computer simulations, comparison between the Enskog theory and MD simulations in the case of the self-diffusion coefficient [15] and kinetic temperatures in a granular mixture [16] have shown good agreement for all α at $n^* \equiv n\sigma^3 \lesssim 0.25$ and for all densities at $\alpha \gtrsim 0.9$. Here, n is the number density and σ is the diameter of spheres. More recent agreement has been found in the case of granular mixtures under shear flow [17]. The Enskog transport coefficients [11] have also been tested against real NMR experiments of a system of mustard seeds vibrated vertically [18,19]. The averaged value of the coefficient of restitution of the grains used in this experiment is $\alpha=0.87$, which lies outside of the quasielastic limit ($\alpha \approx 0.99$). Comparison between theory and experiments (see for instance, Figs. 10-13 of Ref. [19]) shows that the Enskog kinetic theory [11] successfully models the density and granular temperature profiles away from the vibrating container bottom and quantitatively explains the temperature inversion observed in experiments. All these results clearly show the applicability of the Enskog theory for densities outside the Boltzmann limit ($n^* \to 0$) and values of dissipation beyond the quasielastic limit. In this context, one can conclude that the Enskog equation provides a unique basis for the description of dynamics across a wide range of densities, length scales, and degrees of dissipation. No other theory with such generality exists.

The explicit knowledge of the Navier-Stokes transport coefficients as well as of the cooling rate for inelastic hard spheres [11] allows one to solve the linearized hydrodynamic equations around the homogeneous cooling state (HCS) and identify the conditions for stability as functions of the wave vector, the dissipation, and the density. In the low-density limit, previous results derived from the Boltzmann equation are recovered [4]. Linear stability analysis shows two transversal (shear) modes and a longitudinal ("heat") mode to be unstable with respect to long wavelength excitations. The corresponding critical values for the shear and heat modes are also determined, showing that the clustering instability is mainly driven by the transversal shear mode, except for quite large dissipation. As expected, these results agree qualitatively well with those previously derived in Ref. [9]. On the other hand, at a quantitative level, the comparison carried out here shows significant differences between both descriptions as the collisions become more inelastic.

The plan of the paper is as follows. In Sec. II, the basis of the hydrodynamic equations for a dense gas as derived from the (inelastic) Enskog equation is described. The explicit dependence of the transport coefficients and the cooling rate on dissipation is also illustrated for some values of density to show that the influence of inelasticity on transport is in general quite significant. Section III is devoted to the linear stability analysis around the HCS and presents the main results of this paper. The paper is closed in Sec. IV with some concluding remarks.

II. HYDRODYNAMIC DESCRIPTION

We consider a granular fluid composed of smooth inelastic hard spheres of mass m and diameter σ. Collisions are characterized by a (constant) coefficient of normal restitution $0<\alpha\leq 1$. At a kinetic level, all the relevant information on the system is given through the one-particle velocity distribution function, which is assumed to obey the (inelastic) Enskog equation [13]. From it one can easily get the (macroscopic) hydrodynamic equations for the number density $n(\mathbf{r},t)$, the flow velocity $\mathbf{u}(\mathbf{r},t)$, and the local temperature $T(\mathbf{r},t)$ [11]:

$$D_t n + n\nabla \cdot \mathbf{u} = 0, \tag{1}$$

$$\rho D_t \mathbf{u} + \nabla \mathsf{P} = \mathbf{0}, \tag{2}$$

$$D_t T + \frac{2}{3n}(\nabla \cdot \mathbf{q} + \mathsf{P}:\nabla \mathbf{u}) = -\zeta T. \tag{3}$$

In the above equations, $D_t=\partial_t+\mathbf{u}\cdot\nabla$ is the material derivative, $\rho=nm$ is the mass density, P is the pressure tensor, $\mathbf{q}$ is the heat flux, and ζ is the cooling rate due to the energy dissipated in collisions. The practical usefulness of the balance equations (1)–(3) is limited unless the fluxes and the cooling rate are further specified in terms of the hydrodynamic fields and their gradients. The detailed form of the constitutive equations and the transport coefficients appearing in them have been obtained by applying the Chapman-Enskog method [10] to the Enskog equation. To first order in the gradients, the corresponding constitutive equations are [11]

$$P_{ij} = p\delta_{ij} - \eta\left(\nabla_j u_i + \nabla_i u_j - \frac{2}{3}\delta_{ij}\nabla\cdot\mathbf{u}\right) - \gamma\delta_{ij}\nabla\cdot\mathbf{u}, \quad (4)$$

$$\mathbf{q} = -\kappa\nabla T - \mu\nabla n, \quad (5)$$

$$\zeta = \zeta_0 + \zeta_1\nabla\cdot\mathbf{u}. \quad (6)$$

Here, p is the hydrostatic pressure, η is the shear viscosity, γ is the bulk viscosity, κ is the thermal conductivity, and μ is a new transport coefficient not present in the elastic case. The expressions for the pressure, the transport coefficients and the cooling rate can be written in the forms

$$p = nTp^*(\alpha,\phi), \quad \eta = \eta_0\eta^*(\alpha,\phi), \quad \gamma = \eta_0\gamma^*(\alpha,\phi), \quad (7)$$

$$\kappa = \kappa_0\kappa^*(\alpha,\phi), \quad \mu = \frac{T\kappa_0}{n}\mu^*(\alpha,\phi), \quad \zeta_0 = \frac{nT}{\eta_0}\zeta_0^*(\alpha,\phi), \quad (8)$$

where $\eta_0 = 5(mT)^{1/2}/16\sigma^2\pi^{1/2}$ and $\kappa_0 = 15\eta_0/4m$ are the low-density values of the shear viscosity and the thermal conductivity in the elastic limit, respectively. The quantities $p^*, \eta^*, \gamma^*, \kappa^*, \mu^*, \zeta_0^*$, and ζ_1 are dimensionless functions of the coefficient of restitution α and the solid volume fraction $\phi = \pi n\sigma^3/6$. Their explicit expressions are given in the Appendix, and more details can be found in Ref. [11]. For elastic collisions ($\alpha=1$), $\mu^*(1,\phi), \zeta_0(1,\phi)^*$, and $\zeta_1(1,\phi)$ vanish, while the expressions of $\eta^*(1,\phi), \gamma^*(1,\phi)$, and $\kappa^*(1,\phi)$ coincide with those obtained for a dense gas of elastic hard spheres [10]. In the low-density limit ($\phi=0$), $\gamma^*(\alpha,0) = \zeta_1(\alpha,0) = 0$ and the results derived for a dilute granular gas are recovered [4]. As pointed out before, the new transport coefficient μ is not present for elastic collisions and may play an important role to accurately describe some situations of real granular materials, such as a "temperature inversion" observed in vibrofludized systems [19].

The reduced quantities $\eta^*(\alpha,\phi)/\eta^*(1,\phi), \kappa^*(\alpha,\phi)/\kappa^*(1,\phi), \mu^*(\alpha,\phi)$, and $\zeta_1(\alpha,\phi)$ are plotted in Fig. 1 as functions of the coefficient of restitution for three different values of the solid volume fraction ϕ. As said in the Introduction, these quantities, along with the pressure, were assumed to be the same as in the elastic case in the stability analysis carried out in Ref. [9], i.e., $p^*(\alpha,\phi)\to p^*(1,\phi)$, $\eta^*(\alpha,\phi)\to\eta^*(1,\phi)$, $\kappa^*(\alpha,\phi)\to\kappa^*(1,\phi)$, and $\mu^*(\alpha,\phi)=\zeta_1(\alpha,\phi)\to 0$. Figure 1 shows that in general the influence of dissipation on the transport coefficients and the cooling rate is quite significant and so their functional form differs appreciably from their elastic form. This means that the predictions made in Ref. [9] might quantitatively differ from those obtained here as the rate of dissipation increases. This will be confirmed later. We also see that, for a given value of α, $\eta^*(\alpha,\phi)/\eta^*(1,\phi)$ and $\kappa^*(\alpha,\phi)/\kappa^*(1,\phi)$ decrease as the density increases, while the opposite happens in the cases of $\mu^*(\alpha,\phi)$ and $|\zeta_1(\alpha,\phi)|$.

When the expressions of the pressure tensor, the heat flux and the cooling rate are substituted into the balance equations (1)–(3) one gets the corresponding Navier-Stokes (closed) hydrodynamic equations for $n,\mathbf{u}$, and T. They are given by

$$D_t n + n\nabla\cdot\mathbf{u} = 0, \quad (9)$$

$$D_t u_i + (nm)^{-1}\nabla_i p = (nm)^{-1}\nabla_j\left[\eta\left(\nabla_i u_j + \nabla_j u_i - \frac{2}{3}\delta_{ij}\nabla\cdot\mathbf{u}\right) + \gamma\delta_{ij}\nabla\cdot\mathbf{u}\right], \quad (10)$$

$$(D_t + \zeta_0)T + \frac{2}{3n}p\nabla\cdot\mathbf{u} = \frac{2}{3n}\nabla\cdot(\kappa\nabla T + \mu\nabla n) + \frac{2}{3n}\left[\eta\left(\nabla_i u_j + \nabla_j u_i - \frac{2}{3}\delta_{ij}\nabla\cdot\mathbf{u}\right) + \gamma\delta_{ij}\nabla\cdot\mathbf{u}\right] - T\zeta_1\nabla\cdot\mathbf{u}. \quad (11)$$

Note that consistency would require to consider up to second order in the gradients in the expression (6) for the cooling rate, since this is the order of the terms in Eq. (11) coming from the pressure tensor and the heat flux. However, it has been shown for a dilute gas that the contributions from the cooling rate of second order are negligible as compared with the corresponding contributions from Eqs. (4)–(6) [4]. It is assumed here that the same holds in the dense case.

The form of the Navier-Stokes equations (9)–(11) is the same as for a normal fluid, except for the presence of the contributions to the cooling rate ζ_0 and ζ_1 and the new transport coefficient μ in the energy balance equation. Of course, as Fig. 1 clearly illustrates, the values of the transport coefficients are quite different, depending on the value of the coefficient of restitution α.

III. LINEAR STABILITY ANALYSIS

The hydrodynamic equations (1)–(3) admit a simple solution which corresponds to the so-called homogeneous cooling state (HCS). It describes a uniform state with vanishing flow field and a temperature decreasing monotonically in time, i.e.,

$$T(t) = \frac{T(0)}{[1+\zeta_0(0)t/2]^2}. \quad (12)$$

Nevertheless, computer simulations [1,20,21] have shown that the HCS is unstable with respect to long enough wavelength perturbations. To analyze this problem, it is adequate to perform a stability analysis of the nonlinear hydrodynamic

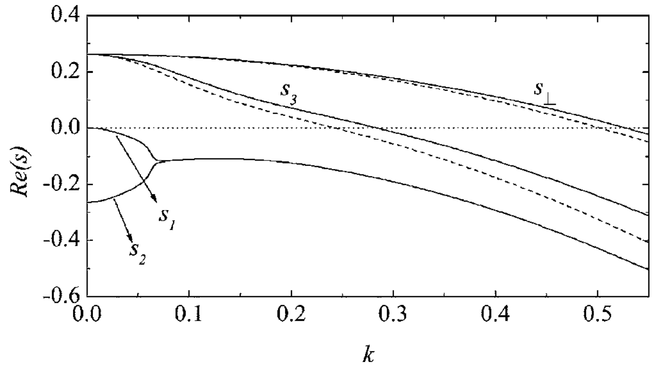

FIG. 2. Dispersion relations for a granular fluid with $\alpha=0.8$ and $\phi=0.2$. From top to bottom the curves correspond to the two degenerate shear (transversal) modes and the remaining three longitudinal modes. The dashed lines correspond to the results obtained for the shear ($s_\perp$) and heat (s_3) modes from the approximations made in Ref. [9]. Only the real parts of the eigenvalues is plotted.

equations (9)–(11) with respect to the homogeneous state for small initial excitations. The linearization of Eqs. (9)–(11) about the homogenous solution yields partial differential equations with coefficients that are independent of space but depend on time since the reference (homogeneous) state is cooling. This time dependence can be eliminated through a change in the time and space variables and a scaling of the hydrodynamic fields.

We assume that the deviations $\delta y_\alpha(\mathbf{r},t)=y_\alpha(\mathbf{r},t)-y_{H\alpha}(t)$ are small, where, $\delta y_\alpha(\mathbf{r},t)$ denotes the deviation of $\{n,\mathbf{u},T,\}$ from their values in the homogeneous state, the latter being denoted by the subscript H. The quantities in the HCS verify

$$\nabla n_H = \nabla T_H = \mathbf{0}, \quad \mathbf{u}_H = \mathbf{0}, \quad \partial_t \ln T_H = -\zeta_{0H}. \tag{13}$$

To recover the results found in the dilute gas case when $\phi \to 0$, I consider the same time and space variables as those used in Ref. [4], namely,

$$\tau = \frac{1}{2}\int_0^t \nu_H(t')dt', \quad \boldsymbol{\ell} = \frac{1}{2}\frac{\nu_H(t)}{v_H(t)}\mathbf{r}, \tag{14}$$

where $\nu_H(t)=\frac{16}{5}n_H\sigma^2\pi^{1/2}v_H(t)$ is an effective collision frequency and $v_H(t)=\sqrt{T_H(t)/m}$. Note that $\nu_H(t)=n_HT_H/\eta_H(1,0)$ is an effective collision frequency associated with the elastic ($\alpha=1$) shear viscosity of a dilute gas ($\phi=0$). The dimensionless time scale τ is the time integral of the average collision frequency and thus is a measure of the average number of collisions per particle in the time interval between 0 and t. The unit length $v_H(t)/\nu_H(t)$ introduced in the second equality of Eq. (14) is proportional to the time-independent mean free path of gas particles.

A set of Fourier transformed dimensionless variables are then introduced by

$$\rho_{\mathbf{k}}(\tau) = \frac{\delta n_{\mathbf{k}}(\tau)}{n_H}, \quad \mathbf{w}_{\mathbf{k}}(\tau) = \frac{\delta \mathbf{u}_{\mathbf{k}}(\tau)}{v_H(\tau)}, \quad \theta_{\mathbf{k}}(\tau) = \frac{\delta T_{\mathbf{k}}(\tau)}{T_H(\tau)}, \tag{15}$$

where $\delta y_{\mathbf{k}\alpha} \equiv \{\delta n_{\mathbf{k}}, \mathbf{w}_{\mathbf{k}}(\tau), \theta_{\mathbf{k}}(\tau)\}$ is defined as

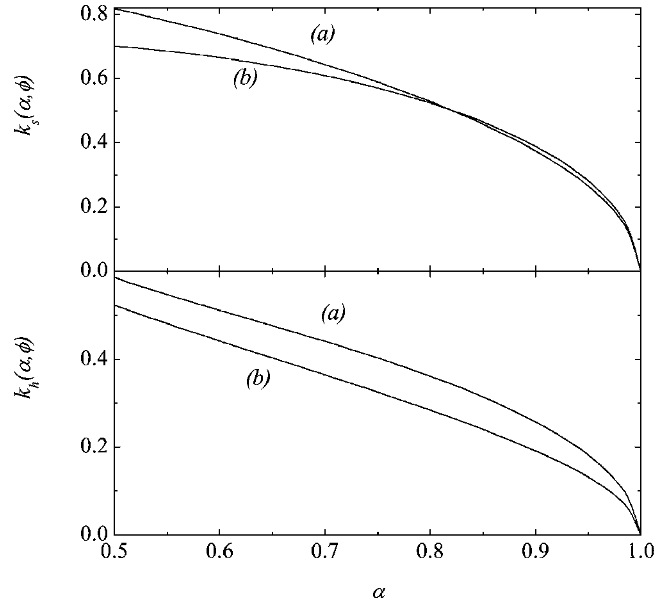

FIG. 3. Plot of the the critical wave numbers $k_s(\alpha,\phi)$ and $k_h(\alpha,\phi)$ as functions of the coefficient of restitution α for two values of the solid volume fraction ϕ: (a) $\phi=0$ and (b) $\phi=0.2$.

$$\delta y_{\mathbf{k}\alpha}(\tau) = \int d\boldsymbol{\ell}\ e^{-i\mathbf{k}\cdot\boldsymbol{\ell}}\delta y_\alpha(\boldsymbol{\ell},\tau). \tag{16}$$

Note that in Eq. (16) the wave vector $\mathbf{k}$ is dimensionless. In terms of the above variables, the transverse velocity components $\mathbf{w}_{\mathbf{k}\perp}=\mathbf{w}_{\mathbf{k}}-(\mathbf{w}_{\mathbf{k}}\cdot\hat{\mathbf{k}})\hat{\mathbf{k}}$ (orthogonal to the wave vector $\mathbf{k}$) decouple from the other three modes and hence can be ob-

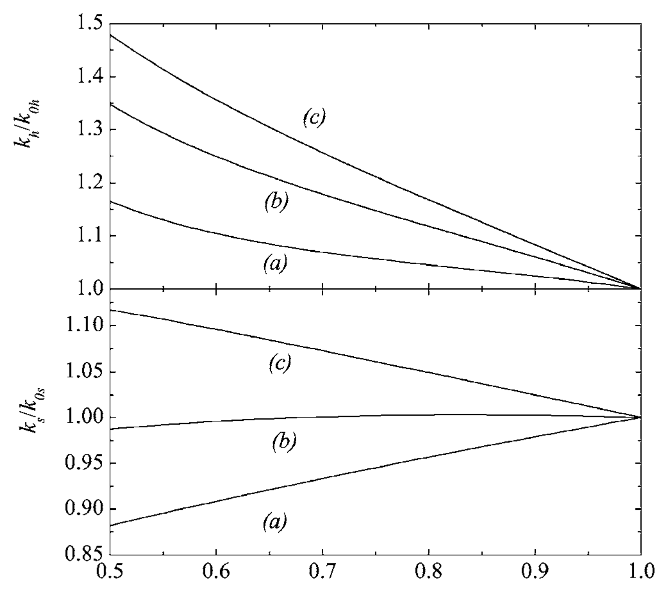

FIG. 4. Plot of the ratios k_s/k_{0s} and k_h/k_{0h} as functions of the coefficient of restitution α for three values of the solid volume fraction ϕ: (a) $\phi=0$, (b) $\phi=0.1$, and (c) $\phi=0.2$. Here, k_{0s} and k_{0h} are the critical wave numbers obtained from the approximations made in Ref. [9].

tained more easily. Their evolution equation is

$$\left(\frac{\partial}{\partial\tau}-\zeta_0^*+\frac{1}{2}\eta^*k^2\right)\mathbf{w}_{\mathbf{k}\perp}=0, \tag{17}$$

where it is understood that ζ_0^* and η^* are evaluated in the HCS. The solution to Eq. (17) is

$$\mathbf{w}_{\mathbf{k}\perp}(\mathbf{k},\tau)=\mathbf{w}_{\mathbf{k}\perp}(0)\exp[s_\perp(k)\tau], \tag{18}$$

where

$$s_\perp(k)=\zeta_0^*-\frac{1}{2}\eta^*k^2. \tag{19}$$

This identifies two shear (transversal) modes analogous to the elastic ones. According to Eq. (19), there exists a critical wave number k_s given by

$$k_s=\left(\frac{2\zeta_0^*}{\eta^*}\right)^{1/2}. \tag{20}$$

This critical value separates two regimes: shear modes with $k>k_s$ always decay while those with $k<k_s$ grow exponentially.

The remaining (longitudinal) modes correspond to $\rho_{\mathbf{k}},\theta_{\mathbf{k}}$, and the longitudinal velocity component of the velocity field, $w_{\mathbf{k}\parallel}=\mathbf{w}_{\mathbf{k}}\cdot\hat{\mathbf{k}}$ (parallel to $\mathbf{k}$). These modes are coupled and obey the equation

$$\frac{\partial\,\delta y_{\mathbf{k}\alpha}(\tau)}{\partial\tau}=M_{\alpha\beta}\delta y_{\mathbf{k}\beta}(\tau), \tag{21}$$

where $\delta y_{\mathbf{k}\alpha}(\tau)$ denotes now the set $\{\rho_{\mathbf{k}},\theta_{\mathbf{k}},w_{\mathbf{k}\parallel}\}$ and M is the square matrix,

$$\mathsf{M}=\begin{pmatrix}0 & 0 & -ik\\ -2\zeta_0^*g-\frac{5}{4}\mu^*k^2 & -\zeta_0^*-\frac{5}{4}\kappa^*k^2 & -\frac{2}{3}ik\left(p^*+\frac{3}{2}\zeta_1\right)\\ -ikp^*C_\rho & -ikp^* & \zeta_0^*-\frac{2}{3}\eta^*k^2-\frac{1}{2}\gamma^*k^2\end{pmatrix}. \tag{22}$$

As before, it is understood that $p^*,\eta^*,\gamma^*,\kappa^*,\mu^*,\zeta_0^*$, and ζ_1 are evaluated in the HCS. In addition, the quantities $g(\phi)$ and $C_\rho(\alpha,\phi)$ are given by

$$g(\phi)=1+\phi\frac{\partial}{\partial\phi}\ln\chi(\phi), \tag{23}$$

$$C_\rho(\alpha,\phi)=1+g(\phi)\frac{p^*(\alpha,\phi)-1}{p^*(\alpha,\phi)}=1+g(\phi)-\frac{g(\phi)}{1+2(1+\alpha)\phi\chi(\phi)}, \tag{24}$$

where in the last equality use has been made of the explicit expression of p^* given by Eq. (A1). In Eqs. (23) and (24), $\chi(\phi)$ is the pair correlation function at contact. In kinetic theory calculations, the value of χ for the pre-collisional distribution is used, which is well approximated by local equilibrium. There are nonequilibrium corrections that can be calculated from the ring collision operator [22]. However, these corrections are very hard to calculate and so for simplicity I take here the Carnahan-Starling approximation [23]:

$$\chi(\phi)=\frac{2-\phi}{2(1-\phi)^3}. \tag{25}$$

In the limit $\phi\to0$, $p^*=g=C_\rho=1$, $\gamma^*=\zeta_1=0$ and Eqs. (17)–(21) reduce to those previously derived for a dilute gas [4].

The longitudinal three modes have the form $\exp[s_n(k)\tau]$ for $n=1$, 2, 3, where $s_n(k)$ are the eigenvalues of the matrix M, namely, they are the solutions of the cubic equation

$$s^3+\frac{5}{4}\left(\kappa^*+\frac{2}{5}\gamma^*+\frac{8}{15}\eta^*\right)k^2s^2+\left\{k^4\kappa^*\left(\frac{5}{6}\eta^*+\frac{5}{8}\gamma^*\right)+k^2\left[p^*C_\rho+\frac{2}{3}\eta^*\zeta_0^*+\frac{1}{2}\gamma^*\zeta_0^*+\frac{1}{3}p^*(2p^*+3\zeta_1)-\frac{5}{4}\kappa^*\zeta_0^*\right]-\zeta_0^{*2}\right\}s+p^*\left[\frac{5}{4}(\kappa^*C_\rho-\mu^*)k^2+\zeta_0^*(C_\rho-2g)\right]k^2=0. \tag{26}$$

As happens for a dilute gas [4], for given values of α and ϕ the analysis of Eq. (26) shows that at very small k all modes are real, while at larger k two modes become a complex conjugate pair of propagating modes. Thus the physical meaning of the longitudinal modes is different from that in the elastic fluids, even when $\alpha\to1$ [4].

The solution to Eq. (26) can be obtained for small k by a perturbation expansion as

$$s_n(k)=s_n^{(0)}+ks_n^{(1)}+k^2s_n^{(2)}+\cdots. \tag{27}$$

Substituting this expansion into Eq. (26) yields $s_1^{(0)}=0$, $s_2^{(0)}=-\zeta_0^*$, $s_3^{(0)}=\zeta_0^*$,

$$s_n^{(1)}=0, \tag{28}$$

$$s_1^{(2)} = \frac{p^*}{\zeta_0^*}(C_\rho - 2g), \tag{29}$$

$$s_2^{(2)} = p^* \frac{2p^* + 3(\zeta_1 + 2g)}{6\zeta_0^*} - \frac{5}{4}\kappa^*, \tag{30}$$

$$s_3^{(2)} = -p^* \frac{2p^* + 3(\zeta_1 - 2g) + 6C_\rho}{6\zeta_0^*} - \frac{2}{3}\eta^* - \frac{1}{2}\gamma^*. \tag{31}$$

In the case of a dilute gas ($\phi \to 0$), the eigenvalues $s_n(k)$ behave as

$$s_1(k) \to -\frac{1}{\zeta_0^*}k^2, \tag{32}$$

$$s_2(k) \to -\zeta_0^* + \left(\frac{4}{3\zeta_0^*} - \frac{5}{4}\kappa^*\right)k^2, \tag{33}$$

$$s_3(k) \to \zeta_0^* - \left(\frac{1}{3\zeta_0^*} + \frac{2}{3}\eta^*\right)k^2. \tag{34}$$

Since the Navier-Stokes hydrodynamic equations are valid to second order in k, the solutions (27)–(31) are relevant to the same order.

As said in the Introduction, although the limitations of the Enskog theory are greater than for elastic systems, comparison with MD simulations [15,16] indicate that it is still accurate for ϕ up to about 0.15 and for α greater than about 0.5. For higher densities the α range is more limited, but even then it captures the relevant qualitative features. For this reason, to illustrate the influence of both density and dissipation on instabilities, densities in the interval $0 \leqslant \phi \leqslant 0.2$ for $0.5 \leqslant \alpha \leqslant 1$ will be considered.

The dispersion relations $s_n(k)$ for a fluid with $\alpha=0.8$ and $\phi=0.2$, as obtained from Eq. (20) and the solutions of the cubic equation (26), are plotted in Fig. 2. Only the real part (propagating modes) of the solutions to Eq. (26) is represented. For comparison, the results for the shear ($s_\perp$) and the longitudinal heat (s_3) modes from the approximations made by van Noije and Ernst [9] are also plotted. These curves can be formally obtained from the results derived in this paper when one takes $\mu^* = \zeta_1 = 0$, and p^*, η^*, γ^*, and κ^* are replaced by their values in the elastic limit [Eqs. (A18)–(A20)]. We observe that the agreement between both sets of results is in general good, the heat mode showing more quantitative discrepancies. Figure 2 also shows that the heat mode is unstable for $k < k_h$, where k_h can be obtained from Eq. (26) when $s=0$. The result is

$$k_h = \sqrt{\frac{4\zeta_0^*(2g - C_\rho)}{5(\kappa^* C_\rho - \mu^*)}}. \tag{35}$$

The dependence of the critical values k_s and k_h on dissipation is illustrated in Fig. 3 for two values of ϕ. For a given value of the coefficient of restitution α, in general the corresponding critical values decrease with increasing density. However, there is a small region of values of $\alpha \gtrsim 0.82$ where the opposite happens in the case of k_s. All the above trends are

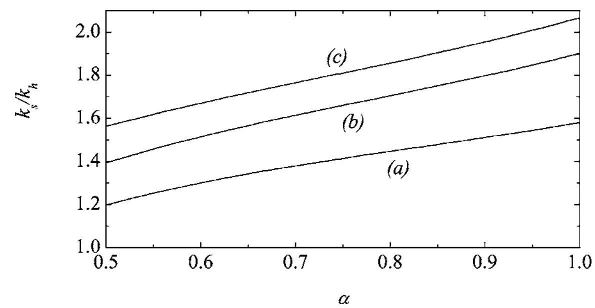

FIG. 5. Ratio k_s/k_h versus the coefficient of restitution α for three values of the solid volume fraction ϕ: (a) $\phi=0$, (b) $\phi=0.1$, and (c) $\phi=0.2$.

also captured by the results obtained in Ref. [9], although quantitative discrepancies between both descriptions appear as the dissipation increases. To illustrate such differences, the ratios k_s/k_{0s} and k_h/k_{0h} are plotted versus α in Fig. 4 for different values of ϕ. Here, k_{0s} and k_{0h} are the critical wave numbers obtained from the approximations made in Ref. [9]. Significant differences between both analyses are clearly shown in Fig. 4, especially for strong dissipation and moderate densities. Thus, for instance, for $\phi=0.2$ and $\alpha=0.8$ the discrepancies between both approaches for k_s and k_h are about 5% and 17%, respectively, while for $\phi=0.2$ and $\alpha=0.5$ the discrepancies are about 12% and 48%, respectively. A more significant qualitative difference between our results and those obtained in Ref. [9] appears in the case of the ratio k_s/k_h. This quantity measures the separation between both critical modes. According to Eqs. (20) and (35), this ratio is independent of α when one neglects the influence of dissipation on the pressure and the transport coefficients. However, the present results predict a complex dependence of k_s/k_h on α. To illustrate it, the ratio k_s/k_h is plotted versus the coefficient of restitution α in Fig. 5 for different values of density. It is apparent that in general both critical values k_s and k_h are well separated, especially for small inelasticity. The results also show that the influence of dissipation on the ratio k_s/k_h is less significant as the system becomes denser. In addition, for a given value of ϕ, there exists a value of the coefficient of restitution $\alpha_0(\phi)$ for which $k_h > k_s$ for values of $\alpha < \alpha_0$. The dependence of α_0 on the solid volume fraction ϕ is plotted in Fig. 6. It is apparent that the value of α_0 decreases with increasing density. However, given that the values of α_0

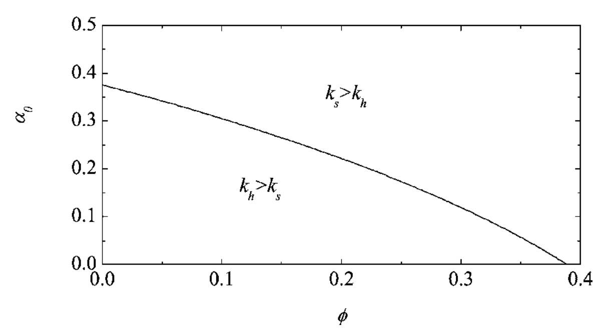

FIG. 6. Dependence of α_0 on the solid volume fraction ϕ. Points above (below) the curve correspond to systems where the instability is driven by the shear (heat) mode.

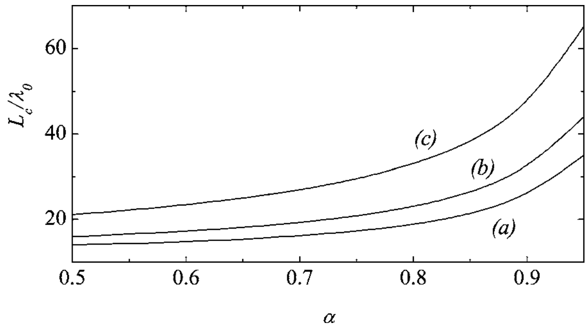

FIG. 7. The critical size L_c in units of the mean free path λ_0 as a function of the coefficient of restitution α for three different values of the solid volume fraction ϕ: (a) $\phi=0$, (b) $\phi=0.1$, and (c) $\phi=0.2$. In each case, the system is linearly stable for points below the corresponding curve.

are quite small, one can conclude that in practice ($\alpha \gtrsim 0.375$) the instability of the system is driven by the transversal shear mode since $k_s > k_h$ for $\alpha > \alpha_0(\phi)$.

According to these results, for not quite extreme values of dissipation ($\alpha \gtrsim 0.375$), three different regions can be identified. For $k > k_s$ all modes are negative and the system is linearly stable with respect to initial perturbations with wave number in this range (short wavelength region). For $k_h < k < k_s$, the shear mode is unstable while the heat mode is linearly stable. In this range the density (coupled to the heat mode) is also stable and so, density inhomogeneities can only be created due to the nonlinear coupling with the unstable shear mode [21]. Finally, if $k < k_s$ first vortices and then clusters are developed and the final state of the system is strongly inhomogeneous. A more detailed analysis of the evolution of the granular gas can be found in Ref. [3].

In a system with periodic boundary conditions, the smallest allowed wave number is $2\pi/L$, where L is the largest system length. Hence, for given values of inelasticity and density, we can identify a critical length L_c so that the system becomes unstable when $L > L_c$. The value of L_c is determined by equating

$$\frac{2\pi}{L_c^*} = \max\{k_s, k_h\}, \quad L_c^* = \frac{\nu_H}{2v_H} L_c. \tag{36}$$

In Fig. 7 we show L_c/λ_0 as a function of α for different values of the solid volume fraction ϕ. Here, $\lambda_0 = (\sqrt{2}\pi n\sigma^2\chi)^{-1} = (5\sqrt{2\pi}\chi/16)^{-1} v_H/\nu_H$ is the mean free path of a hard-sphere dense gas. In all of these systems, $k_s > k_h$ and so

$$L_c = \frac{5}{4}\pi\sqrt{\pi}\chi\sqrt{\frac{\eta^*}{\zeta_0^*}}\lambda_0. \tag{37}$$

For a given value of α, we see that the critical size (in units of the mean free path) increases with density. As a consequence, larger systems are required to observe the shearing instability as the fluid becomes denser.

IV. CONCLUDING REMARKS

A well-known feature of rapid granular flows is the instability of the homogeneous cooling state against long wavelength spatial perturbations, leading to cluster and vortex formation. Although the origin of this instability has been widely explored by using computational tools, prior analytical work on this subject has been limited to weak inelasticity or very dilute regime. In order to gain some insight into the influence of both density and dissipation on the stability of the HCS, a kinetic theory description has been adopted. For moderate densities, the inelastic Enskog equation [13] can be considered as a valuable tool for granular media. As in the case of elastic collisions, the Enskog equation takes into account spatial correlations through the pair correlation function but neglects the velocity correlations between the particles that are about to collide (molecular chaos). The latter assumption has been clearly shown to fail for inelastic collisions as the density increases [14], so that the limitations of the Enskog description are greater than for elastic collisions. Due to this molecular chaos breakdown, some authors conclude that the Enskog equation can be insufficient to compute average properties of inelastic fluids, except for very weak dissipation. Nevertheless, this conclusion contrasts with previous comparisons made with MD simulations [15–17] and with real experiments [18] where, at least for the problems studied there, velocity correlations do not seem to play an important role and the Enskog equation provides quite good estimates for the transport properties of the system. It is remarkable that its accuracy is not restricted to the quasielastic limit since it covers values of moderate density ($0 \leqslant \phi \lesssim 0.15$) and large values of dissipation ($0.5 \lesssim \alpha \leqslant 1$). It is possible that for situations more complex than those analyzed in Refs. [15–19], velocity correlations become important and the Enskog theory does not give reliable predictions. In this case, new kinetic theories incorporating the effect of velocity correlations are needed to describe granular flows. However, so far there is no alternative to the Enskog theory for finite density systems at this point. Hence it is the most accurate theory to describe systems of interest in simulations and experiments.

In this paper I have used the inelastic Enskog kinetic theory to perform a linear stability analysis of the hydrodynamic equations and identify the conditions for stability in terms of dissipation and density. The analysis is based on a previous derivation [11] of the expressions of the Enskog transport coefficients and the cooling rate that, *a priori*, is not limited to small dissipation. This is the main different ingredient of this work since previous studies [9] on linear stability analysis for dense granular gases considered weakly inelastic systems and so, thermodynamic and transport properties were assumed to be the same as those of *elastic* hard sphere fluids. However, this assumption is expected to fail as dissipation increases since the form of the *inelastic* transport coefficients clearly differs from their elastic counterparts, as shown for instance in Fig. 1.

The study reported here extends to higher densities a previous linear stability analysis performed for a dilute gas [4]. In general, the findings agree qualitatively well with previous results [9], showing that the effect of dissipation on transport coefficients do not significantly modify the qualitative form of the dispersion relations. Specifically, linear stability analysis shows two unstable modes: a transversal shear mode and a longitudinal heat mode. The instability of both modes is a long wavelength instability. The analysis of the dependence of the corresponding critical shear wave number k_s [defined in Eq. (20)] and heat wave number k_h [defined in Eq. (35)] shows that, except for extreme values of dissipation, the instability is driven by the transversal shear mode. The range of values of the coefficient of restitution α for which $k_h > k_s$ is shortened as the gas becomes denser. Thus, for $\phi \gtrsim 0.389$, $k_s > k_h$ for any value of α.

On the other hand, as expected, quantitative discrepancies between our results and those given in Ref. [9] become significant as the dissipation increases. In particular, at a given value of density, the critical wave numbers k_s and k_h are in general underestimated (except in the case of k_s for a low-density gas) when one neglects the influence of inelasticity on transport [9] while the ratio k_s/k_h (which is independent of the coefficient of restitution α in Ref. [9]) presents a complex dependence on the rate of dissipation, as is illustrated in Fig. 5. Therefore although the description made by van Noije and Ernst [9] predicts reasonably well the dispersion relations as well as the long-range structure, one expects that the results reported here improve such predictions when one considers values of the coefficient of restitution α for which transport properties are clearly affected by the rate of dissipation.

As said in the Introduction, in the case of a dilute gas ($\phi=0$) comparison with direct Monte Carlo simulation of the Boltzmann equation has shown the accuracy of the stability analysis performed in Ref. [4]. Given that the results reported here extends the above description to high densities, comparison with MD simulations becomes practical. In this context, it is hoped that the description reported here stimulates the performance of such computer simulations to characterize the onset and evolution of the clustering instability. As in the Boltzmann case [7,24], one expects that the Enskog results describes accurately the first stages of evolution.

Finally, it must noted that all the results obtained in this paper has been made in the context of a very simple collision model where the coefficient of restitution is constant. Recent results [25] derived with an impact-velocity-dependent coefficient of restitution shows that structure formation occurs in free granular gases only as a transient phenomenon, whose duration increases with the system size.

ACKNOWLEDGMENTS

I am grateful to Dr. James Lutsko for pointing out some errors in the evaluation of the terms coming from the cooling rate to first order in the gradients. Partial support of the Ministerio de Educación y Ciencia (Spain) through Grant No. FIS2004-01399 (partially financed by FEDER funds) is acknowledged.

APPENDIX

In this Appendix, the expressions for the hydrostatic pressure, the transport coefficients and the cooling rate used in Eqs. (4)–(8) are given. The reduced hydrostatic pressure p^* is

$$p^* = 1 + 2(1+\alpha)\phi\chi. \tag{A1}$$

The reduced transport coefficients $\eta^*, \gamma^*, \kappa^*$, and μ^* defined through the relations (7) and (8) are given, respectively, by

$$\eta^* = \eta_k^*\left[1 + \frac{4}{5}\phi\chi(1+\alpha)\right] + \frac{3}{5}\gamma^*, \tag{A2}$$

$$\gamma^* = \frac{128}{5\pi}\phi^2\chi(1+\alpha)\left(1 - \frac{c}{32}\right), \tag{A3}$$

$$\kappa^* = \kappa_k^*\left[1 + \frac{6}{5}\phi\chi(1+\alpha)\right] + \frac{256}{25\pi}\phi^2\chi(1+\alpha)\left(1 + \frac{7}{32}c\right), \tag{A4}$$

$$\mu^* = \mu_k^*\left[1 + \frac{6}{5}\phi\chi(1+\alpha)\right]. \tag{A5}$$

Here, the superscript k denotes the contributions to the transport coefficients coming from the kinetic parts of the fluxes [11]. These kinetic contributions are

$$\eta_k^* = \left(\nu_\eta^* - \frac{1}{2}\zeta_0^*\right)^{-1}\left[1 - \frac{2}{5}(1+\alpha)(1-3\alpha)\phi\chi\right], \tag{A6}$$

$$\kappa_k^* = \frac{2}{3}(\nu_\kappa^* - 2\zeta_0^*)^{-1}\left\{1 + [1+(1+\alpha)\phi\chi]c + \frac{3}{5}\phi\chi(1+\alpha)^2 \times\left[2\alpha - 1 + \left(\frac{1+\alpha}{2} - \frac{5}{3(1+\alpha)}\right)c\right]\right\}, \tag{A7}$$

$$\mu_k^* = 2(2\nu_\kappa^* - 3\zeta_0^*)^{-1}\left\{(1 + \phi\partial_\phi \ln\chi)\zeta_0^*\kappa_k^* + \frac{1}{3}p^* \times(1 + \phi\partial_\phi \ln p^*)c - \frac{4}{5}\phi\chi(1+\alpha)\left(1 + \frac{1}{2}\phi\partial_\phi \ln\chi\right) \times\left[\alpha(1-\alpha) + \frac{1}{4}\left(\frac{4}{3} + \alpha(1-\alpha)\right)c\right]\right\}. \tag{A8}$$

In these expressions, c, ζ_0^*, ν_η^*, and ν_κ^* are functions of α and ϕ given by

$$c = \frac{32(1-\alpha)(1-2\alpha^2)}{81 - 17\alpha + 30\alpha^2(1-\alpha)}, \tag{A9}$$

$$\zeta_0^* = \frac{5}{12}\chi(1-\alpha^2)\left(1 + \frac{3}{32}c\right), \tag{A10}$$

$$\nu_\eta^* = \chi\left[1 - \frac{1}{4}(1-\alpha)^2\right]\left(1 - \frac{c}{64}\right), \tag{A11}$$

$$\nu_\kappa^* = \frac{1}{3}\chi(1+\alpha)\left[1 + \frac{33}{16}(1-\alpha) + \frac{19-3\alpha}{1024}c\right]. \tag{A12}$$

Furthermore, in three dimensions the Carnahan-Starling approximation [23] for the the pair correlation function at contact $\chi(\phi)$ is given by

$$\chi(\phi) = \frac{2-\phi}{2(1-\phi)^3}. \tag{A13}$$

The coefficient ζ_1 appearing in the expression (6) for the cooling rate ζ is

$$\zeta_1 = \left[\frac{5}{32}\left(1+\frac{3}{64}c\right)c_\zeta - 2\right]\phi\chi(1-\alpha^2), \tag{A14}$$

where [26]

$$c_\zeta = \frac{\frac{4}{15}\lambda + (1+\alpha)\left(\frac{1}{3}-\alpha\right)c}{\nu_\zeta^* - \frac{5}{8}(1-\alpha^2)\left(1+\frac{3}{32}c\right) + \frac{5c}{64}\left(1+\frac{3}{64}c\right)(1-\alpha^2)}, \tag{A15}$$

$$\nu_\zeta^* = \frac{1+\alpha}{192}\left(241 - 177\alpha + 30\alpha^2 - 30\alpha^3 + \frac{c}{64} \times (30\alpha^3 - 30\alpha^2 + 2001\alpha - 1873)\right) \tag{A16}$$

$$\lambda = \frac{3}{8}(1+\alpha)\left((1-\alpha)(5\alpha^2+4\alpha-1) + \frac{c}{12} \times (159\alpha + 3\alpha^2 - 19 - 15\alpha^3)\right). \tag{A17}$$

For elastic collisions ($\alpha=1$), $c=\zeta_0^*=\mu^*=\zeta_1=0$ and

$$p^*(1,\phi) = 1 + 4\chi\phi, \quad \gamma^*(1,\phi) = \frac{256}{5\pi}\chi\phi^2, \tag{A18}$$

$$\eta^*(1,\phi) = \chi^{-1}\left(1+\frac{8}{15}\chi\phi\right)^2 + \frac{3}{5}\gamma^*, \tag{A19}$$

$$\kappa^*(1,\phi) = \chi^{-1}\left(1+\frac{12}{5}\chi\phi\right)^2 + \frac{2}{5}\gamma^*. \tag{A20}$$

These expressions coincide with well-know results derived for normal hard-sphere fluids [10].

[1] I. Goldhirsch and G. Zanetti, Phys. Rev. Lett. **70**, 1619 (1993).
[2] S. McNamara, Phys. Fluids A **5**, 3056 (1993).
[3] N. Brilliantov and T. Pöschel, *Kinetic Theory of Granular Gases* (Oxford University Press, Oxford, 2004).
[4] J. J. Brey, J. W. Dufty, C. S. Kim, and A. Santos, Phys. Rev. E **58**, 4638 (1998).
[5] J. W. Dufty and J. J. Brey, Phys. Rev. E **68**, 030302(R) (2003).
[6] J. W. Dufty, A. Baskaran, and L. Zogaib, Phys. Rev. E **69**, 051301 (2004); J. W. Dufty and J. J. Brey, cond-mat/0410133.
[7] J. J. Brey, M. J. Ruiz-Montero, and F. Moreno, Phys. Fluids **10**, 2976 (1998).
[8] I. Goldhirsch, M-L. Tan, and G. Zanetti, J. Sci. Comput. **8**, 1 (1993); P. Deltour and J. L. Barrat, J. Phys. I **7**, 137 (1997); R. Brito and M. H. Ernst, Europhys. Lett. **43**, 497 (1998); Int. J. Mod. Phys. C **9**, 1339 (1998); S. Luding and H. J. Herrmann, Chaos **9**, 25 (1999).
[9] T. P. C. van Noije and M. H. Ernst, Phys. Rev. E **61**, 1765 (2000).
[10] S. Chapman and T. G. Cowling, *The Mathematical Theory of Nonuniform Gases* (Cambridge University Press, Cambridge, England, 1970).
[11] V. Garzó and J. W. Dufty, Phys. Rev. E **59**, 5895 (1999).
[12] V. Garzó and J. M. Montanero, Physica A **313**, 336 (2002).
[13] J. J. Brey, J. W. Dufty, and A. Santos, J. Stat. Phys. **87**, 1051 (1997).
[14] S. McNamara and S. Luding, Phys. Rev. E **58**, 2247 (1998); R. Soto and M. Mareschal, *ibid.* **63**, 041303 (2001); R. Soto, J. Piasecki, and M. Mareschal, *ibid.* **64**, 031306 (2001); I. Pagonabarraga, E. Trizac, T. P. C. van Noije, and M. H. Ernst, *ibid.* **65**, 011303 (2002).
[15] J. Lutsko, J. J. Brey, and J. W. Dufty, Phys. Rev. E **65**, 051304 (2002).
[16] S. R. Dahl, C. M. Hrenya, V. Garzó, and J. W. Dufty, Phys. Rev. E **66**, 041301 (2002).
[17] M. Alam and S. Luding, J. Fluid Mech. **476**, 69 (2003); J. M. Montanero, V. Garzó, M. Alam, and S. Luding, cond-mat/0411548.
[18] X. Yang, C. Huan, D. Candela, R. W. Mair, and R. L. Walsworth, Phys. Rev. Lett. **88**, 044301 (2002).
[19] C. Huan, X. Yang, D. Candela, R. W. Mair, and R. L. Walsworth, Phys. Rev. E **69**, 041302 (2004).
[20] S. McNamara and W. R. Young, Phys. Rev. E **50**, R28 (1994); **53**, 5089 (1996).
[21] J. J. Brey, M. J. Ruiz-Montero, and D. Cubero, Phys. Rev. E **60**, 3150 (1999).
[22] J. F. Lutsko, Phys. Rev. E **63**, 061211 (2001).
[23] N. F. Carnahan and K. E. Starling, J. Chem. Phys. **51**, 635 (1969).
[24] J. J. Brey, M. J. Ruiz-Montero, and D. Cubero, Europhys. Lett. **48**, 359 (1999).
[25] N. Brilliantov, C. Salueña, T. Schwager, and T. Pöschel, Phys. Rev. Lett. **93**, 134301 (2004).
[26] As noted before, some errors occur in the expression given in Ref. [11] for the coefficient c_ζ. The expressions given here corrects such results.